Continuous Plug Flow and Discrete Particle Phase Coupling Using Triangular Parcels

Anders Schou Simonsen, Thomas Condra, Kim Sørensen

Abstract—Various processes are modelled using a discrete phase, where particles are seeded from a source. Such particles can represent liquid water droplets, which are affecting the continuous phase by exchanging thermal energy, momentum, species etc. Discrete phases are typically modelled using parcel, which represents a collection of particles, which share properties such as temperature, velocity etc. When coupling the phases, the exchange rates are integrated over the cell, in which the parcel is located. This can cause spikes and fluctuating exchange rates.

This paper presents an alternative method of coupling a discrete and a continuous plug flow phase. This is done using triangular parcels, which span between nodes following the dynamics of single droplets. Thus, the triangular parcels are propagated using the corner nodes. At each time step, the exchange rates are spatially integrated over the surface of the triangular parcels, which yields a smooth continuous exchange rate to the continuous phase.

The results shows that the method is more stable, converges slightly faster and yields smooth exchange rates compared with the steam tube approach. However, the computational requirements are about five times greater, so the applicability of the alternative method should be limited to processes, where the exchange rates are important. The overall balances of the exchanged properties did not change significantly using the new approach.

Keywords—CFD, coupling, discrete phase, parcel.

I. INTRODUCTION

VARIOUS processes can be simplified by assuming plug flow, when the geometry is fairly simple. Such can be flows in tubes, where the changes in the radial direction can be assumed uniform, which is a common approximation within the field of chemistry. Although the approximation has some deficiencies, it will captures the overall tendencies in [1]. The plug flow approximation can also be used in other processes, where the radial changes can be assumed uniform without loosing much accuracy, which is the case for sprayer based scrubbers. Such serve to remove chemical compounds from an exhaust gas by spraying water counter stream of the gas phase [2]. Modelling such a phenomena requires a discrete phase, where droplet particles are injected into the continuous phase.

Modelled processing involving both continuous and discrete phases are typically coupled, which ensures transfer of energy, mass, momentum etc. The continuous phase is modelled by discretizing the domain into a number of cells, which

Anders Schou Simonsen is with the Department of Energy Technology, Aalborg University, Denmark (e-mail: asi@et.aau.dk).

Thomas Condra is with the Department of Energy Technology, Aalborg University, Denmark (e-mail: tc@et.aau.dk).

Kim Sørensen is with the Department of Energy Technology, Aalborg University, Denmark (e-mail: kso@et.aau.dk).

hold information about the continuous flow field such as temperature, velocity, pressure etc. In case of plug flow, only the axial direction is discretized, where each cell has uniform properties in the radial direction.

The discrete phase is modelled by injecting a number of droplets into the flow field. A typical injection point with a *Rosin-Rammler distribution* [3] will inject $10^7 \ \mathrm{droplets/(kg/s)}$, which would be computationally inefficient, if all were to be tracked. Instead, the droplets are modelled using parcels, where each of these represents a collection of droplets, which are sharing properties [4]. The parcels move according to the local flow field, where the trajectory will be similar to that of a single droplet within the parcel. When coupling the discrete phase with the continuous phase, the parcels exchange properties with the cells, in which they are located over time. Thus, the exchange rates between the phases are computed using the surface area flow rate for each parcel, as most rates are linearly dependent of this such as heat and mass transfer. The surface area flow rate is simply the surface area for a single droplet multiplied by the number of droplets within the parcel itself.

When coupling the two phases, the exchange rates are integrated in time, and the transferred properties are then adjusted in the parcels and cells in order to ensure conservation of mass and energy. However, a large number of parcels is required for accurate flow modelling, which can be computationally expensive, as each parcel does only interact with the current cell, in which it is located. Several methods exists, where the influence area for each parcel is adjusted in order to model the actual phenomena.

Stochastic particle tracking allows the parcels to be affected by the turbulent fluctuations within the continuous phase [5]. By solving the trajectories for each parcel multiple times, a representative number of paths will be available, where the exchange rates are distributed over a large number of cells, which coincide with the trajectories. Another method is to use cloud tracking, where each parcel is initialized with a finite diameter of influence [5]. By integrating the turbulent continuous variables over time, the influence diameter is allowed to grow. As such, a mean trajectory is obtained along with a diameter of influence over which the exchange rates can be calculated and integrated in order to couple the two phases. Diffusive smoothing of the exchange rates is a third approach, where a single trajectory is solved for each parcel, and the resulting exchange rates are distributed over the neighbouring cells by diffusive smoothing [6]. All the above mentioned models are methods to reduce the parcel count and some to

World Academy of Science, Engineering and Technology
International Journal of Mechanical and Mechatronics Engineering
Vol:12, No:9, 2018

include the effects of turbulence.

This paper describes a method for coupling a discrete and a continuous phase, where the parcels are represented by triangular surfaces rather than stream-tubes. The surfaces are propagated by allowing the nodes to move in the flow field. This method allows for surface integration of the exchange rates, where all cells intersecting the surface will get a contribution of the overall exchange rate. This help to smooth out the exchange rates, which will mimic the rates experienced as the number of parcels tends towards infinity.

II. DISCRETE PHASE

When modelling a discrete phase, a number of parcels are typically injected from a point source. Each parcel represents a finite number of particles, which share properties such as position, velocity, temperature etc. The spatial location is governed by particle dynamics, where the surrounding properties of the continuous phase are interpolated and used to calculate the accelerations of the parcels. The equations governing particle dynamics are shown in (1) assuming spherical particles [7].

$$
\begin{aligned}
\vec{v}_{\text{Rel}} &= [\dot{x}, \dot{y}, \dot{z} - \widetilde{v}] \\
Re &= \frac{d \cdot |\vec{v}_{\text{Rel}}| \, \widetilde{\rho}}{\widetilde{\mu}} \\
C_{\text{D}} &= \frac{24}{Re} \cdot \left(1 + 0.15 \cdot Re^{0.681}\right) + \frac{0.407}{1 + 8710/Re} \\
\vec{F} &= \frac{1}{2} \cdot \widetilde{\rho} \cdot |\vec{v}_{\text{Rel}}|^2 \cdot (r^2 \cdot \pi) \cdot C_{\text{D}} + m \cdot \vec{g} \\
\ddot{x} &= F_{\text{x}}/m \\
\ddot{y} &= F_{\text{y}}/m \\
\ddot{z} &= F_{\text{z}}/m
\end{aligned}
\tag{1}
$$

The spatial location of each parcel is denoted with x, y and z. The variables with a tilde are the continuous flow variables, which are interpolated at the positions of the parcels. Note that d, r and m are representing the diameter, radius and mass respectively for a single particle within the parcel. The exchanged properties between the continuous and discrete phases can be both mass, energy etc., where this paper will focus on energy. The governing equations with respect to thermal energy are shown in (2) [8].

$$
\begin{aligned}
Nu &= 2 + \left(0.4 \cdot \sqrt{Re} + 0.06 \cdot Re^{2/3}\right) \cdot \widetilde{Pr}^{0.4} \\
h &= \frac{Nu \cdot \widetilde{k}}{d} \\
Q &= h \cdot \left(4 \cdot \pi \cdot r^2\right) \cdot \left(T - \widetilde{T}\right)
\end{aligned}
\tag{2}
$$

A. Injection Point

A typical injection point is a nozzle, which distributes the parcels over a large area with various droplet sizes according to some distribution. This paper will only deal with a single droplet size for simplicity, and a discussion of this will follow at the end of the article. A hollow cone sprayer can be seen in Fig. 1, where the injection points are distribution on the

surface of a spherical segment and each vector is a normal on the spherical surface. Only half of the sprayer surface has been shown, as symmetry is utilized in this paper.
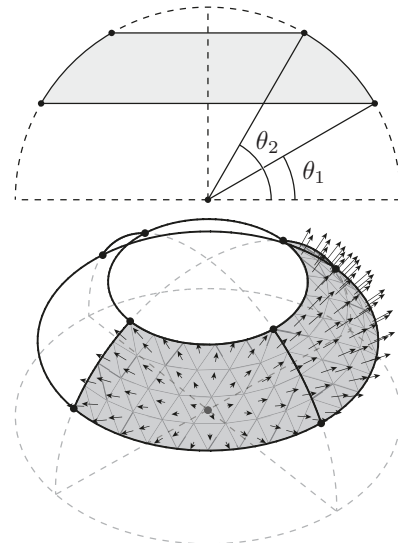

Fig. 1 A hollow cone sprayer represented by a spherical segment. The surface is triangulated, where each incenter has an outward pointing normal vector. The shown sprayer has $\theta_1 = 30°$ and $\theta_2 = 60°$, which results in 75 nodes, n_{N}, and 112 faces, n_{F}

The sprayer surface is triangulated and the normal vectors are located at the incenter of each triangle, which is defined as the intersection of the angle bisectors. The parcels will be injected in the direction of the normal vectors, and each parcel is initialized with some associated mass flow. This paper uses the area fraction of each triangle to distribute the total mass flow to each parcel. The droplet number count in each parcel can be calculated by dividing with the mass of a single droplet. This has been shown in (3) for the ith parcel, where the thermal energy rate within each parcel is denoted $\dot{H}_{\text{i}}$.

$$
\begin{aligned}
\dot{m}_{\text{i}} &= \frac{A_{\text{i}}}{\sum_{\text{i}=1}^{n_{\text{F}}} A_{\text{i}}} \cdot \frac{\dot{m}_{\text{Total}}}{2} \\
m_{\text{Drop}} &= \rho \cdot \frac{4}{3} \cdot \pi \cdot r^3 \\
\dot{N}_{\text{i}} &= \frac{\dot{m}_{\text{i}}}{m_{\text{Drop}}} \\
\dot{A}_{\text{Surf,i}} &= \dot{N}_{\text{i}} \cdot \left(4 \cdot \pi \cdot r^2\right) \\
\dot{H}_{\text{i}} &= \dot{m}_{\text{i}} \cdot c_{\text{p,L}} \cdot T_{\text{i}} \\
\dot{Q}_{\text{i}} &= h \cdot \dot{A}_{\text{Surf,i}} \cdot \left(T_{\text{i}} - \widetilde{T}_{\text{i}}\right) = Q \cdot \dot{N}_{\text{i}}
\end{aligned}
\tag{3}
$$

$\dot{m}_{\text{Total}}$ is the total mass flow of the sprayer, which is divided by two in order to reflect symmetry. Notice that $\dot{A}_{\text{Surf,i}}$ is the surface area rate or the parcel, which can be seen as the total surface area flowing through a cross section of each parcel trajectory or steam tube. Thus, when calculating the thermal energy rate, $\dot{Q}_{\text{i}}$, this will use $\dot{A}_{\text{Surf,i}}$, which convert the units from W to W/s.

World Academy of Science, Engineering and Technology
International Journal of Mechanical and Mechatronics Engineering
Vol:12, No:9, 2018

B. Phase Coupling

In order to accurately model a phenomena combining both a discrete and a continuous phase, these must be coupled. As previously stated, this paper will only deal with the transfer of thermal energy. Assuming plug flow in the continuous phase, where the properties only changes in a single spatial dimension, namely the axial z-direction, the exchange rate can be expressed according to (4), where $\mathcal{H}$ is the *Heaviside function*. Both a continuous and discrete version of the thermal energy transfer has been shown in (4), where $\widetilde{q}_j$ is the energy rate per unit volume for the jth cell. $\widetilde{q}_{j,\text{Con}}$ and $\widetilde{q}_{j,\text{Dis}}$ are the continuous and discrete versions of the same equation respectively. This will later be implemented as a source term, when the continuous phase thermal energy is updated iteratively, thus changing the temperature of the gas phase. n_t is the number of discrete time steps. (4) has been illustrated in Fig. 2.

$$\Delta \widetilde{V}_j = (\widetilde{z}_{j,1} - \widetilde{z}_{j,0}) \cdot \widetilde{A}_{\text{Cross}}$$

$$\Phi_j(z) = \mathcal{H}(z - \widetilde{z}_{j,0}) \cdot \mathcal{H}(\widetilde{z}_{j,1} - z)$$

$$\widetilde{q}_{j,\text{Con}} = \frac{1}{\Delta \widetilde{V}_j} \sum_{i=1}^{n_F} \int_0^{t_{\text{Sim}}} \dot{Q}_i(t) \cdot \Phi_j(z_i(t)) \, \mathrm{d}t \quad (4)$$

$$\widetilde{q}_{j,\text{Dis}} = \frac{1}{\Delta \widetilde{V}_j} \sum_{i=1}^{n_F} \sum_{it=1}^{n_t} \dot{Q}_{i,it} \cdot \Phi_j(z_{i,it}) \cdot \Delta t$$

The auxiliary function, $\Phi_j(z)$, is unity when $\widetilde{z}_{j,0} \leq z \leq \widetilde{z}_{j,1}$ and zero otherwise, where the limits indicate the lower and upper z-coordinates of the jth cell. $\widetilde{A}_{\text{Cross}}$ is the cross sectional area of the continuous phase.

The energy rates from two parcels to the continuous phase cells have been shown in the graph to the right in Fig. 2. It can be seen that the energy rates are largest at the top parts of the parcel trajectories, where they are spending the most time compared with the other cells. Also, the parcels are heated over time, and thus decreasing the driving temperature differences and implicitly the thermal energy rates.

When injecting the parcels using the described method, various problems exists. One is that the sprayer surface is not fully represented. In between the parcels, a relatively large area is not represented, as the parcels are acting like stream tubes, in which the droplets are moving. Also, the edges of the sprayer surface is not represented in any way, which will increase as the parcel count is reduced.

Another inconsistency is the spikes in the energy rates to the continuous phase. As seen in Fig. 2, $\widetilde{q}$ fluctuates at every z-direction extrema of the trajectories. This causes spikes in the energy rate, where a continuous and smooth exchange rate is expected. This can somewhat be corrected by smoothing out the exchange rates, which can be done in a manner, which conserves energy. However, the accuracy is lost, as it might not represent the actual phenomena.

This paper will deal with the above mentioned shortcomings by representing the parcels using the triangulation of the sprayer shown in Fig. 1, which allows for surface integrations of the exchange rates. This will in turn yield a smooth and
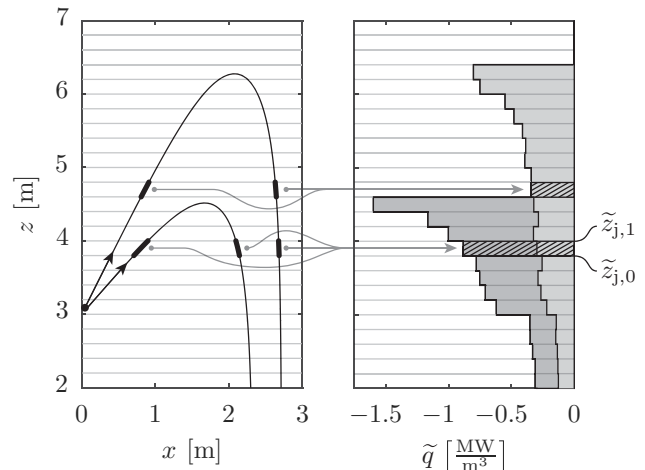

Fig. 2 The coupling between the phases shown illustratively. Each cell receives thermal energy according to the location of the parcels in the z-direction, where only two parcels have been shown. The jth cell has been highlighted, which is enclosed by $\widetilde{z}_{j,0}$ and $\widetilde{z}_{j,1}$, where both parcels are contributing to the energy rate. $\widetilde{q}$ is negative as it is seen from the continuous phase, which is cooled by the droplets

continuous energy rate to the cells in the continuous phase, while fully representing the sprayer surface area.

C. Face-Parcels and Tri-Parcels

The proposed method involved representing the parcels as surfaces instead of steam tubes. The surfaces will be constructed using the nodes of the triangulation, which maintain the connectivity throughout the simulation. This has been shown in Fig. 3, where face-parcels refers to the previously described method and tri-parcels refers to the proposed method. The dashed lines represent the trajectories of droplets being injected from the black vectors. The face-parcels are injected at the incenter of the triangles, whereas the tri-parcels are propagated according to the trajectories of the corner points, which obey the same dynamics as the face-parcels shown in (1). As such, the complete surface of the sprayer is represented by the tri-parcels. The propagated triangles will store properties such as temperature, mass etc. Triangular surfaces are chosen as these will always remain planer, which is not the case for quadrilaterals and more complex shapes.
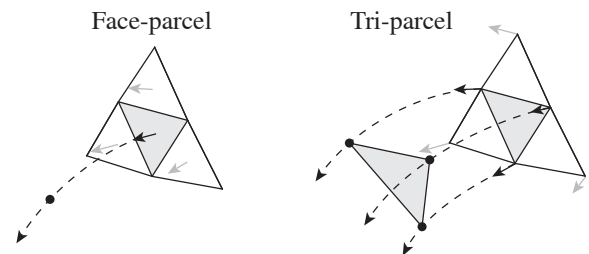

Fig. 3 The face-parcels are injected at the incenter of the triangles, and the tri-parcels are spatially propagated using the nodes of the triangles, which move according to (1)

World Academy of Science, Engineering and Technology
International Journal of Mechanical and Mechatronics Engineering
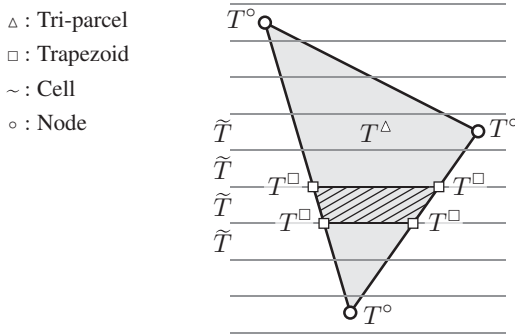Vol:12, No:9, 2018

Fig. 4 The notation used to describe the method of evaluating the surface integrals on each tri-parcel. The notations will be applied as superscripts, where the temperature, T, has been given as an example above. The horizontal lines represents the cells in the continuous phase
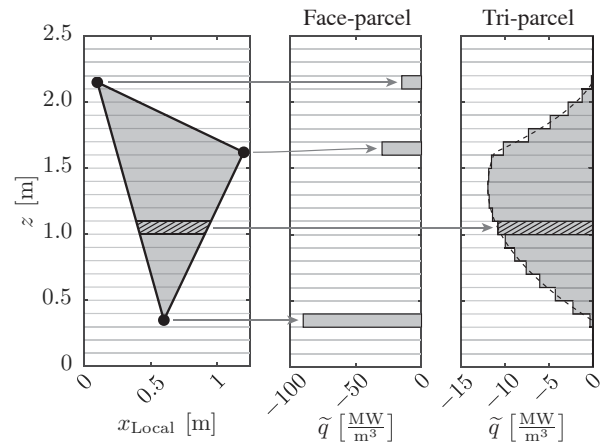

Fig. 5 A tri-parcel at a given time step shown the left graph. The middle graph is the exchange rates, if only the nodes were used, which is an analogue to the face-parcels. The right most graph is showing the exchange rates, when surface integrals are applied

The integration method shown in (4) and Fig. 2 cannot be used to integrate the exchange rates between the discrete and continuous phases for the tri-parcels, as the properties to be exchanged are represented on the triangular surfaces. Thus, surface integrals are required in order to compute the exchange rates.

In order to describe the method of evaluating the surface integrals, the nomenclature shown in Fig. 4 will be used. The superscripts are shown in the legend in the upper left corner of the figure, where these will be used to denote where the properties are located. Tri-parcel properties are stored at the surfaces, and node properties at the corners of each tri-parcel. Trapezoid properties are interpolated in between the node properties, and cell properties are stored in the continuous gas phase.

III. Surface Integrals

When coupling the tri-parcels with the continuous phase, surface integrals must be evaluated in order to calculate the exchange rates. As such, (4) must be formulated in a manner, which is applicable to tri-parcels. This has been shown in (5) and illustratively in (5).

$$\widetilde{q}_j = \frac{1}{\Delta \widetilde{V}_j} \sum_{i=1}^{n_F} \int_0^{t_{Sim}} \int_{\widetilde{z}_{j,0}}^{\widetilde{z}_{j,1}} \overbrace{\frac{\partial \dot{Q}_i^\Delta(z,t)}{\partial A_i(z)^\Delta}}^{\text{Specific exchange rate}} \Bigg|_{z=z_i(t)} \cdot \Phi_j(z_i(t)) \cdot \frac{dA_i^\Delta(z)}{dz} \, dz \, dt$$
(5)

The integral in (5) for the jth cell is evaluated in between the enclosing z-coordinates, $\widetilde{z}_{j,0}$ and $\widetilde{z}_{j,1}$. Conservation of energy has been obeyed, so the integral of $\widetilde{q}(z)$ from 0 to $2.5\,\text{m}$ in Fig. 5 are equal for the face- and tri-parcel.

Fig. 5 also shows the apparent spikes in the continuous phase exchange rates, if face-parcels are used. Notice that the figure is showing the exchange rates in between two time steps, so they are representing the time integrated values of (5) from t_n to t_{n+1}. If the exchange rates from the face-parcels are simply put into their corresponding continuous cell, three distinctive spikes will form. However, using tri-parcels instead yields a smooth and continuous exchange rate to the cells.

It should be noted that the face-parcels follows trajectories, which are injected from the incenter and not the nodes, so the figure is simply showing face-parcels to be located at the tri-parcel nodes for illustration purposes. The dashed line in the right most graph is the exchange rate as $n_{\text{Cells}} \to \infty$.

In order to perform the surface integrals, several steps are required. These are executed at every time step and have been listed below:

A) Calculate weighted properties at the tri-parcel nodes
B) Split each tri-parcel at the mid node and interpolate node properties
C) Subdivide each sub triangle at the intersections with the cells
D) Integrate over subdivided surfaces analytically and sum these to their corresponding cell

The different steps listed above will be explained in details in the following subsections.

A. Weighted Node Properties

The surface integrals can be made assuming a constant average exchange rate for each tri-parcel. This would imply that the term labelled *Specific exchange rate* in (5) is constant for each tri-parcel. However, this would lead to inaccurate representation of the actual phenomena, as the location of the tri-parcels nodes can be in different locations, where the driving temperature differences might be different. This would most likely imply different specific exchange rates at each node, which would cause the term labelled *Specific exchange rate* to vary as a function of z.

Instead of assuming a constant specific exchange rate, the properties required to calculate the exchange rates are allowed to change linearly on the surface of the tri-parcel. For heat transfer these are the droplet surface areas, the heat transfer coefficient and the driving temperature difference according to *Newton's law of cooling*. The linearly varying properties on

World Academy of Science, Engineering and Technology
International Journal of Mechanical and Mechatronics Engineering
Vol:12, No:9, 2018

the surface of each tri-parcel are found by calculating averaged properties at the nodes. This is done by area averaging the properties of all tri-parcels connected to each specific node. In order to conserve energy and mass, the averaging process sums one third of the neighbouring properties, which has been shown in (6) for all properties related to heat transfer. The area weighting has been shown illustratively in Fig. 6 as well.

$$\dot{H}_i^\circ = \sum_{j=1}^{n_{NB}} \frac{\dot{H}_j^\triangle}{3}$$

$$\dot{m}_i^\circ = \sum_{j=1}^{n_{NB}} \frac{\dot{m}_j^\triangle}{3}$$

$$\dot{N}_i^\circ = \sum_{j=1}^{n_{NB}} \frac{\dot{N}_j^\triangle}{3} \quad (6)$$

$$\dot{A}_{Surf,i}^\circ = \dot{N}_i^\circ \cdot \left(4 \cdot \pi \cdot r^2\right)$$

$$T_i^\circ = \frac{\dot{H}_i^\circ}{\dot{m}_i^\circ \cdot c_{p,L}}$$

$$\Delta T_i^\circ = \widetilde{T}_i^\circ - T_i^\circ$$

n_{NB} is the number of neighbouring tri-parcels for the ith node, where j loops over the correct indices corresponding to the neighbours. Keep in mind that the superscripts corresponds to different locations according to Fig. 4. Notice that only the conserving properties are summed. The heat transfer coefficient is independent of the conserving properties, and is calculated directly at the nodes, where the velocities are stored as well. As such, (1) applies for the heat transfer coefficient.

As multiple variables are to be calculated using the same weighting, a sparse matrix can be assembled, which acts as shown in (7). ϕ is one of the conserving properties, $\dot{H}$, $\dot{m}$ or $\dot{N}$.

$$[\mathbf{K}] \cdot [\phi^\triangle] = [\phi^\circ]$$

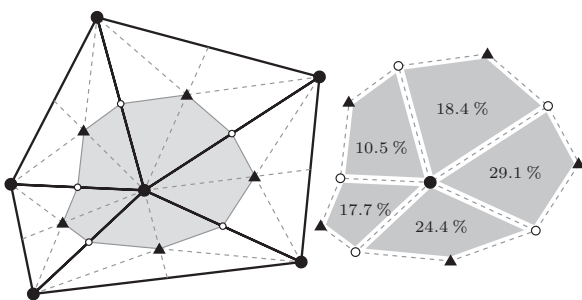$$\sum_{i=1}^{n_F} \phi_i^\triangle = \sum_{i=1}^{n_N} \phi_i^\circ \quad (7)$$

Fig. 6 The area weighted properties of the nodes are calculated using the neighbouring tri-parcels. The centroids are shown as small triangles, the midpoints as white circles and the nodes as solid circles. The highlighted area for each tri-parcel is equal to one third of the respective areas. The right image is showing the relative influence by the neighbouring tri-parcels on the node itself in the given example, where $n_{NB} = 5$

$[\mathbf{K}]$ has size $(n_N \times n_F)$, and $[\phi^\triangle]$ and $[\phi^\circ]$ have sizes $(n_F \times 1)$ and $(n_N \times 1)$ respectively. The conserving property of the weighting has been shown in the bottom of (7).

B. Midpoint Split

The second step is to split each triangle into two at the middle node in the z-direction. This has been shown in Fig. 7, where the node numbered 2 is chosen for splitting, as it is the middle node. The intersection point on the opposite edge of node 2 will be denoted $2'$, and new properties are linearly interpolate here using the properties of node 1 and 3 according to (8).

$$\phi_{2'}^\circ = (\phi_3^\circ - \phi_1^\circ) \cdot \frac{z_{2'}^\circ - z_1^\circ}{z_3^\circ - z_1^\circ} \quad (8)$$
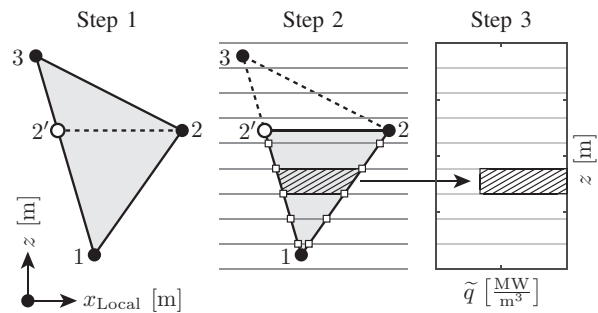

Fig. 7 The three main steps shown visually. Step 1 splits the tri-parcel at the middle node in the z-direction. Step 2 subdivides the new sub triangles according to the intersections with the continuous cells. Step 3 sums the energy rate from each sub trapezoid to the corresponding cells in the continuous phase

The following steps requires the horizontal length of the new segment, which is found by (9). $x_{2'}^\circ$ and $y_{2'}^\circ$ are calculated with (8) by substituting ϕ with either x or y.

$$\Delta L_{2-2'} = \sqrt{(x_2^\circ - x_{2'}^\circ)^2 + (y_2^\circ - y_{2'}^\circ)^2} \quad (9)$$

C. Subdivision

All triangles are now split in two at the midpoint lines, which creates twice the number of triangles. However, each of the new triangles will have an edge aligned with the x-y-plane between their local node 2 and $2'$. These new triangles can now be subdivided at the intersections with the cell of the continuous phase, which has been shown in Fig. 7 as the white squares. The properties at all intersections are linearly interpolated using the node values on the edges, which are node 1, 2 and $2'$ in the example. The new subdivided surfaces consists of trapezoids and a a single triangle at node 1. A trapezoid has been shown in Fig. 8, where the superscript $\square$ is used. Triangles are represented as having either L_0 or L_1 equal to zero, which generalizes the method, as the same equations can be used for both shapes.
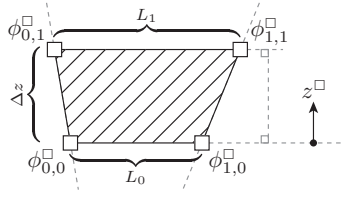
World Academy of Science, Engineering and Technology
International Journal of Mechanical and Mechatronics Engineering
Vol:12, No:9, 2018

Fig. 8 A subdivided trapezoidal with interpolated values at its local corners, $\phi^\square$. L_0 and L_1 are the lengths of the edges and Δz is the height of the trapezoid. $z^\square$ is the local coordinate system in the z-direction

D. Surface Integration

Each trapezoid has interpolated value for both ΔT and h at the corners. The geometry is also fully defined, so a surface integral can be evaluated in order to calculate the area weighted average of the product $\Delta T \cdot h$. Bilinear interpolation is used to find the values in between the four corners, which is shown in (10) [9].

$$\Delta L(z) = L_0 + (L_1 - L_0) \cdot \frac{z^\square}{\Delta z}$$

$$\phi(x, z^\square) = \frac{[\Delta L(z) - x, x]}{\Delta L(z) \cdot \Delta z} \cdot \begin{bmatrix} \phi_{0,0}^\square & \phi_{0,1}^\square \\ \phi_{1,0}^\square & \phi_{1,1}^\square \end{bmatrix} \cdot \begin{bmatrix} \Delta z - z^\square \\ z^\square \end{bmatrix}$$
(10)

Notice that bilinear interpolation can be performed using the local coordinate system of each trapezoid, as the surface is planar. The average value of the product between $\Delta T \cdot h$ can be evaluated by surface integrating over the trapezoid and dividing by the trapezoid area, $A_i^\square$. Once again, this is independent of the coordinate system as long as the horizontal edges are aligned with the x-y-plane. This has been shown in (11).

$$A_i^\square = \int_0^{\Delta z} \int_0^{\Delta L(z)} 1 \, dx \, dz$$

$$\overline{\Delta T \cdot h} = \frac{\int_0^{\Delta z} \int_0^{\Delta L(z)} \Delta T(x, z) \cdot h(x, z) \, dx \, dz}{A_i^\square}$$

$$\overline{\Delta T \cdot h} = \frac{1}{36 \cdot (L_0 + L_1)} \cdot$$
(11)

$$\left(\begin{bmatrix} T_{0,0}^\square \\ T_{0,1}^\square \\ T_{1,0}^\square \\ T_{1,1}^\square \end{bmatrix}^\mathrm{T} \cdot \left(\begin{bmatrix} 6 & 2 & 3 & 1 \\ 2 & 2 & 1 & 1 \\ 3 & 1 & 6 & 2 \\ 1 & 1 & 2 & 2 \end{bmatrix} \cdot \begin{bmatrix} h_{0,0}^\square \\ h_{0,1}^\square \\ h_{1,0}^\square \\ h_{1,1}^\square \end{bmatrix} \right) \cdot L_0 + \right.$$

$$\left. \begin{bmatrix} T_{0,1}^\square \\ T_{0,0}^\square \\ T_{1,1}^\square \\ T_{1,0}^\square \end{bmatrix}^\mathrm{T} \cdot \left(\begin{bmatrix} 6 & 2 & 3 & 1 \\ 2 & 2 & 1 & 1 \\ 3 & 1 & 6 & 2 \\ 1 & 1 & 2 & 2 \end{bmatrix} \cdot \begin{bmatrix} h_{0,1}^\square \\ h_{0,0}^\square \\ h_{1,1}^\square \\ h_{1,0}^\square \end{bmatrix} \right) \cdot L_1 \right)$$

The average product, $\overline{\Delta T \cdot h}$, can now be multiplied with the total droplet surface area going through the trapezoid, $\dot{A}_{\mathrm{Surf,i}}^\square$, which will imply the energy rate between the continuous and discrete phase. The exchange area for the ith trapezoid located in the jth cells, $q_{j,i}^\square$, can be found by (12).

$$\dot{A}_{\mathrm{Surf,i}}^\square = \dot{A}_{\mathrm{Surf,i}}^\triangle \cdot \frac{A_i^\square}{A_i^\triangle}$$

$$q_{j,i}^\square = \frac{1}{\Delta \widetilde{V}_j} \cdot \overline{\Delta T \cdot h} \cdot \dot{A}_{\mathrm{Surf,i}}^\square \cdot \Delta t$$
(12)

As the thermal energy rates for all trapezoids have been calculated, these can be summed for each cell to calculate the total exchange rate to continuous phase. This has been shown in (13).

$$\widetilde{q}_j = \sum_{i=1}^{n_{\mathrm{F}}} q_{j,i}^\square$$
(13)

When the specific energy rates to all cells has been found, the temperature can be calculated using (14) and (15), which are the continuous and discrete versions of the same equations respectively.

$$\widetilde{H}_j = \widetilde{H}_{\mathrm{Inlet}} + \Delta \widetilde{V} \cdot \sum_{i=1}^{j} \widetilde{q}_i$$

$$\widetilde{T}_j = \frac{\widetilde{H}_j}{c_{\mathrm{p,G}} \cdot \widetilde{m}}$$
(14)

$$\widetilde{H}(z) = \widetilde{H}_{\mathrm{Inlet}} + \widetilde{A}_{\mathrm{Cross}} \cdot \int_0^z \widetilde{q}(z) \, dz$$

$$\widetilde{T}(z) = \frac{\dot{\widetilde{H}}(z)}{c_{\mathrm{p,G}} \cdot \widetilde{m}}$$
(15)

IV. RESULTS

In order to evaluating the performance of the proposed method, a test case is used to compare the two methods. This case will consist of a plug flow model, where droplets are seeded from a hollow cone sprayer. The droplets will move according to the local flow field, where density, velocity and viscosity is taken into account. The droplets will be seeded with an initial temperature, which causes them to transfer energy to and from the continuous gas phase. This will in turn cause the temperature of the continuous phase to change, thus affecting the density, velocity, viscosity, conductivity etc. A steady state solution can be obtained by an iterative numerical method, which has been shown in Fig. 9.

The implementation is done in *MATLAB*, where the code has been streamlined to be as efficient as possible for a fair comparison of the computational requirements.

A. Continuous Phase

The geometry will be a simple tube with an inlet at the bottom and an outlet at the top. The domain is divided into a number of cells, n_{Cells}, which are spaced equally along the z-direction. The continuous phase will be represented by these cells, where
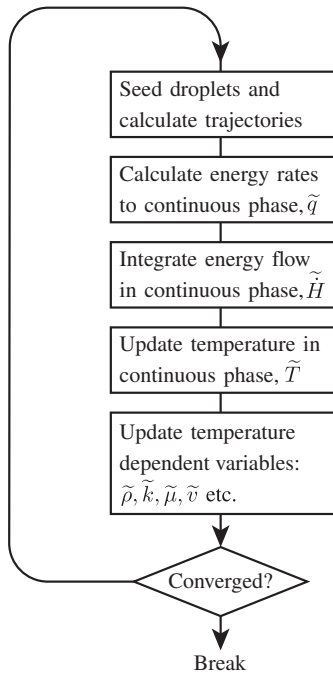
World Academy of Science, Engineering and Technology
International Journal of Mechanical and Mechatronics Engineering
Vol:12, No:9, 2018

Fig. 9 A subdivided trapezoidal with interpolated values at its local corners, $\phi^\square$. L_0 and L_1 are the lengths of the edges and Δz is the height of the trapezoid. $z^\square$ is the local coordinate system in the z-direction
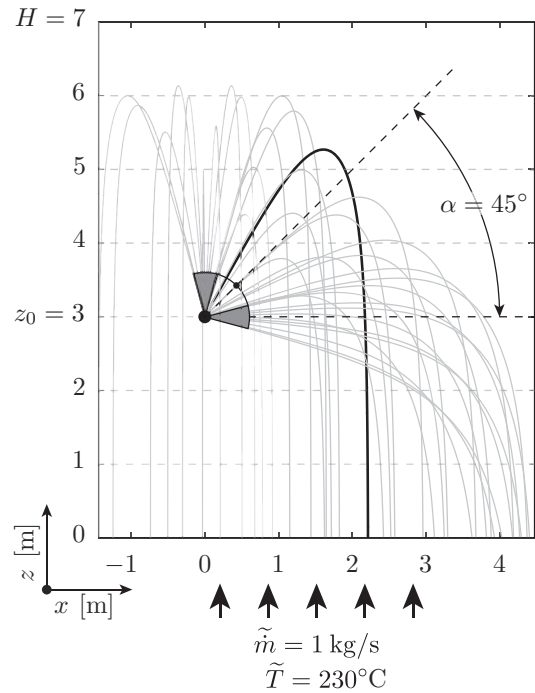

Fig. 10 A sketch of the domain, which is divided into a number of cells, n_{Cells}. Droplets are being seeded from the nozzle and move according to the local flow field. Thermal energy is transferred in between the two phases

the flow properties do not change with the radial coordinate, thus plug flow. A sketch of the domain has been shown in Fig. 10, where a number of droplets are seeded and move according to the local flow field. Notice that the parcels are not constrained in the radial direction, as collision with the walls is not taken into account for simplicity.

The correlations and constants used for the continuous gas phase are listen in Tab. I. All properties can be derived from $\widetilde{m}$, $\widetilde{D}$ and $\widetilde{T}$, where the latter will vary when thermal energy is transferred to and from the discrete droplet phase, thus affecting the local flow field properties and indirectly

TABLE I
THE CONSTANTS AND CORRELATIONS OF THE GAS PHASE. NOTICE THAT THE CORRELATED POLYNOMIALS FOR μ AND k ARE ONLY VALID WITHIN $0°C \leq T \leq 250°C$

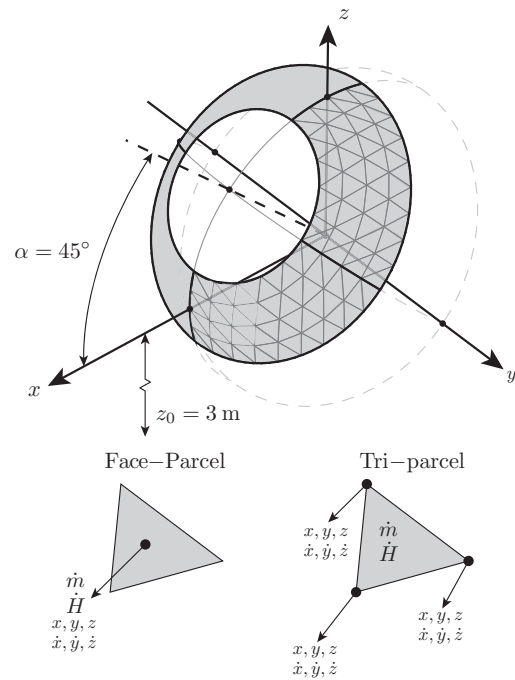| Property	Symbol	Value
Mass flow	$\widetilde{m}$	$1\ \frac{\text{kg}}{\text{s}}$
Temperature	$\widetilde{T}_{\text{Inlet}}$	$230°C$
Diameter	D	$1\ \text{m}$
Area	$\widetilde{A}_{\text{Cross}}$	$0.785\ \text{m}^2$
Velocity	$\widetilde{v}$	$\widetilde{m}/\left(\widetilde{\rho} \cdot \widetilde{A}_{\text{Cross}}\right)$
Molar weight	MW	$28.97 \cdot 10^{-3}\ \frac{\text{kg}}{\text{mol}}$
Gas heat capacity	$c_{\text{p,G}}$	$1025\ \frac{\text{J}}{\text{kg·K}}$
Liquid heat capacity	$c_{\text{p,L}}$	$4192\ \frac{\text{J}}{\text{kg·K}}$
Pressure	$\widetilde{P}$	$101325\ \text{Pa}$
Density	$\widetilde{\rho}$	$MW \cdot \widetilde{P}/\left(R \cdot \left(\widetilde{T} + 273.15\ \text{K}\right)\right)$
Viscosity	$\widetilde{\mu}$	$\left(17.22\text{e}{-6} + 4.1967\text{e}{-8} \cdot \frac{\widetilde{T}}{\text{K}}\right) \cdot \frac{\text{kg}}{\text{m·s}}$
Conductivity	$\widetilde{k}$	$\left(0.02436 + 6.7\text{e}{-5} \cdot \frac{\widetilde{T}}{\text{K}}\right) \cdot \frac{\text{W}}{\text{m·K}}$
Prandtl number	$\widetilde{Pr}$	0.7

Fig. 11 The hollow cone sprayer used for the comparison along with a legend of where the properties are stored for the two methods

the droplet trajectories and heat transfer rates. As such, the problem is non-linear.

World Academy of Science, Engineering and Technology
International Journal of Mechanical and Mechatronics Engineering
Vol:12, No:9, 2018

B. Discrete Phase

The nozzle will be similar to the shown in Fig. 1 with angles of $\theta_1 = 30°$ and $\theta_2 = 60°$. The node count, n_N, will be varied in the analysis and thus also the number of triangular faces, n_F. The cone will be inclined with $\alpha = 45°$ upwards towards the outlet and have an initial velocity magnitude of 15 m/s. The total mass flow will be 0.5 kg/s and will be distributed over the tri-parcels according to the surface areas as previously described. The initial liquid temperature will be $10°\text{C}$. The sprayer in the test case has been shown in Fig. 11. In the lower part of the same figure, an illustration has been shown of where the parcel properties are stored during simulation using the two different methods to be compared.

C. Comparison

The comparison will be divided into three parts. The first is to compare a base case, where the number of parcels, n_F, is kept constant along with the number of cells, n_{Cells}. The second part will be comparing the methods when changing n_{Cells}, whereas the third part will change n_F. All simulations will be carried out until all droplets/parcels have exited the domain at $z = 0$, which takes around 4 s. The time step will be $\Delta t = 1 \text{ ms}$.

1) Base Case: The base case will compare the energy rates between the phases. A hollow cone is generated with the same specifications as previously described, but only consisting of 8 nodes and 6 faces. The continuous domain is divided into 100 cells. This case is made in order to exaggerate the pros and cons of the methods. The results can be seen in Fig. 12.

The results shown in Fig. 12 is showing the energy rate per unit volume between the two phases, $\widetilde{q}$. It can be seen that $\widetilde{q}$ is largest at $z = 3.0 \text{ m}$, where the discrete phase is injected. A consequence of the low parcel count is that the face-parcel method yields a fluctuating energy rate, when compared with the tri-parcels method. The figure to the right is smooth despite the low parcel count. By integrating the energy rates according to (15) the temperature can be obtained
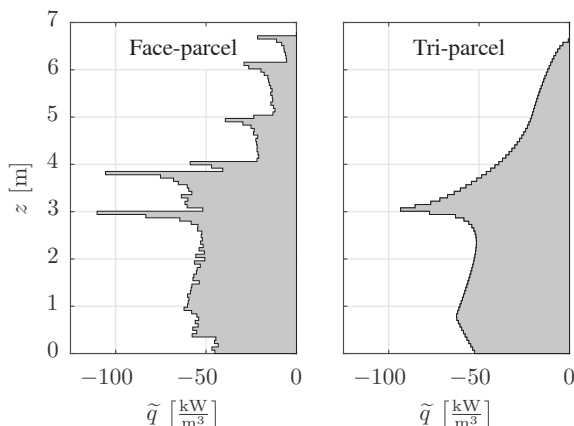
throughout the continuous domain. This has been shown in Fig. 13.

It can be seen that the temperatures of the two methods follow each other closely, though the tri-parcel method is more smooth compared with the face-parcel method. The outlet temperature at $z = 7.0 \text{ m}$ is 85.5 and $86.2 °\text{C}$ for the face- and tri-parcel methods respectively, which is a relatively large difference. This outlet temperatures will be used in the following analyses to compare the two methods as well.

2) Cell Change: This analysis serves to compare the two methods as the number of cell is changed, n_{Cells}. The analysis will be carried out with the sprayer represented with $n_F = 101$ and $n_N = 68$, so the results are almost independent of the parcel count. n_{Cells} has been varied from 20 to 250, where the results can be seen in Fig. 14.

Fig. 14 is showing the outlet temperature of the continuous domain as a function of n_{Cells}. It can be seen that there is a small difference between the two methods of about 0.01 K, so when compared to the absolute temperature difference from the inlet to the outlet, the relative difference is $(0.01 \text{ K}) / ((230 - 86.5) \text{ K}) = 0.007 \%$, so the difference is negligible. It can however be seen that the rate at which the graphs settle at a final value is different. The tri-parcel method settles slightly faster, which was found by fitting an exponential decaying function to the data. These functions can be seen in the figure, where the settling constants are 18.33 and 14.84 cells for the face- and tri-parcel methods respectively. Also, the tri-parcel method has less fluctuations, thus yielding a more stable method. However, as the absolute temperature fluctuations are so small, the effect is minor, but the results are only used for comparing the methods.

3) Parcel Change: This analysis investigates the outlet temperature of the two methods when changing the number of parcels, n_F, from 8 to 251. The number of cells will be held constant at $n_{Cells} = 100$. The results can be seen in Fig. 15.

As seen in the figure, the number of parcels, n_F, does not affect the outlet temperature significantly after ≈ 75, and the largest difference in the outlet temperatures from $n_F \gtrsim 50$ is
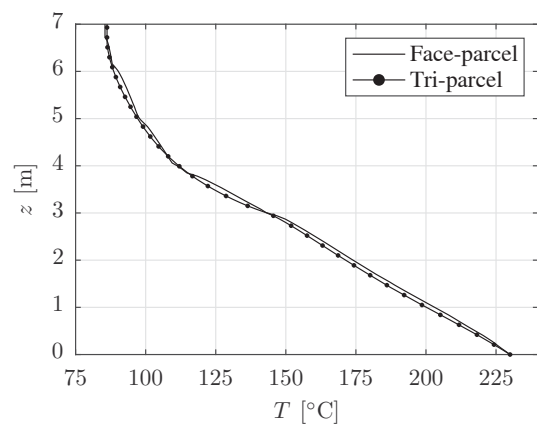
Fig. 12 A comparison between the energy rates per unit volume for the base case. $\widetilde{q}$ fluctuated using the face-parcel method, whereas it is smooth using the tri-parcel method despite the low parcel count

Fig. 13 The temperature of the continuous domain using the two methods. The final temperatures at $z = 7 \text{ m}$ are almost equal
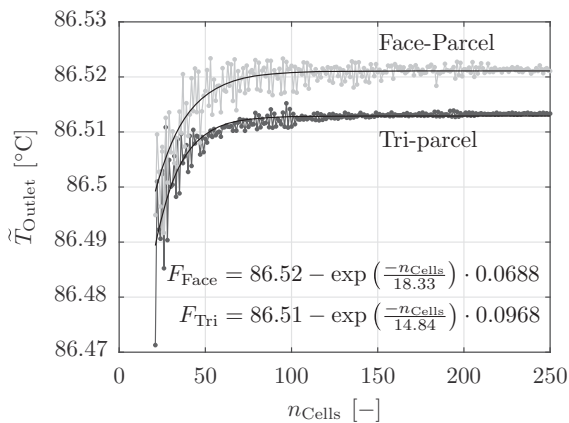
World Academy of Science, Engineering and Technology
International Journal of Mechanical and Mechatronics Engineering
Vol:12, No:9, 2018

Fig. 14 The outlet temperature as a function of n_{Cells} with a constant number of parcels, $n_{\mathrm{F}} = 101$. Exponential decaying functions have been fitted to the results in order to determine the settling time for the two methods
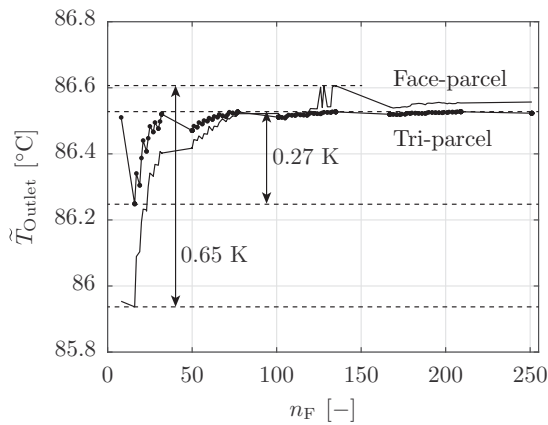

Fig. 15 The outlet temperature as a function of the parcel count, n_{F}, with a constant number of cells, $n_{\mathrm{Cells}} = 100$

about $0.1\ \mathrm{K}$. The tri-parcel method is also closer to its final value at low values of n_{F}, which is seen by the spans of 0.65 and $0.27\ \mathrm{K}$ for the face- and tri-parcel methods respectively. The fluctuations are also smaller using the tri-parcel method, where the outlet temperature is almost constant after ≈ 75.

4) Computational Requirements: The computational requirements were investigated by timing the execution of the two methods. The code has been optimized in Matlab using its profiler [10], where the time consumption of each part of the code is analysed, after which the code can be optimized. As such, the comparison between the two methods should be fair. Based on numerous simulations, the relative difference in computational time was computed. The results showed that the computational requirements using the tri-parcel method was about five times greater compared with the face-parcel method. This difference is primarily caused by the number of interpolations required using the tri-parcel method, which is computationally expensive.

V. Discussion

A. Multiple Droplet Sizes

When seeding liquid droplets as a discrete phase, multiple droplet sizes will usually be present. These typically follows some predefined distribution, where the Rosin-Rammler distribution is common. This distribution correlates the mass fraction with the droplet size. When modelling multiple droplet sizes, each injection point will seed multiple parcels, each with a different droplet size. Some of these droplets might flow upwards and other downwards dependent on their size. The tri-parcel method can be applied to such cases as well by constructing tri-parcels, which are spanning in between different sized droplets. This has been illustrated in Fig. 16.
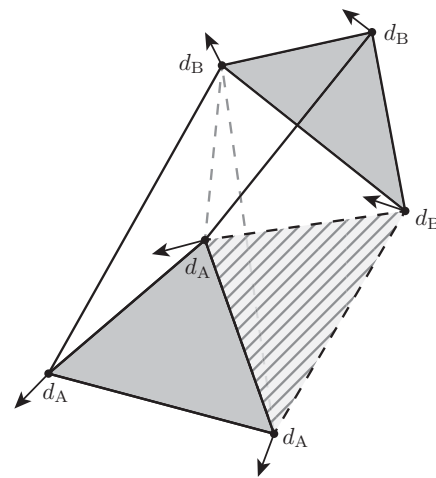

Fig. 16 An illustration of the tri-parcel method, when using multiple droplet sizes. The arrows are indicating the direction of the nodes and the textured area is indicating the tri-parcel, which is spanning between the different sized droplets

Two different sizes of droplets have been shown in Fig. 16, d_{A} and d_{B}, where all droplets with a diameter of d_{A} are falling downwards and d_{B} are flowing upwards. As the formulation of the exchange rates are based on bilinear interpolation of the conserving properties, along with the surface area rate through each trapezoid, the previously stated equations can directly be used to model multiple droplet sizes.

B. Unstructured Mesh Implementation

This paper has focused on plug flow, where the properties of the continuous phase are constant in the radial direction. However, when coupling discrete has continuous phases though computational fluid dynamics, CFD, the mesh will vary in all directions. This complicates the use of tri-parcels, as each parcel would have to be split at each intersection with a cell face. This would be very computationally demanding, although the exchange rates would be smoothed out in a similar manner as the plug flow models.

VI. Conclusion

Two methods have been compared for coupling a continuous and a discrete phase. A basic stream tube approach was used as

World Academy of Science, Engineering and Technology
International Journal of Mechanical and Mechatronics Engineering
Vol:12, No:9, 2018

a baseline, where parcels were interacting with the continuous phase at its current position. This method can cause spikes and fluctuating exchange rates, which the second method addresses.

The alternative method described in this paper represents the parcels as triangular surfaces, tri-parcels. These surfaces are spatially propagated using the corner nodes of the tri-parcels, which move according to the governing equations of particle dynamics. At each time step, the surfaces of the tri-parcels are split and subdivided, after which bilinear interpolation is used to evaluate the surface integral. After the exchange rates have been calculated for each subdivided surface, these can be summed for each cell in the continuous phase. The resulting exchange rate was found to be smooth and continuous.

The results showed that the tri-parcel method proved to be more stable and converged slightly faster, when compared with the stream tube approach. However, the computational requirements were found to be about five times greater for the tri-parcels, as numerous interpolations were required using the alternative method. The overall comparison between the two method did not yield a large difference, where the outlet temperature was investigated. As such, the alternative method is not advantageous, if only the overall characteristics is of interest. However, if the exchange rates are important, the tri-parcel method provides better results, which yields more accurate and realistic results.

REFERENCES

[1] E. A. Foumeny and H. Pahlevanzadeh, *Evaluation of Plug Flow Assumption in Packed Beds*, Chemical Engineering & Technology, Volume 13, Issue 1, 1990.

[2] K. Brown and W. Kalata and Rudolf Schick, *Optimization of SO2 Scrubber using CFD Modeling*, Procedia Engineering, Volume 83, 2014, Pages 170-180.

[3] A. G. Bailey and W. Balachandran and T. J. Williams, *The Rosin-Rammler size distribution for liquid droplet ensembles*, Journal of Aerosol Science, Volume 14, Issue 1, 1983, Pages 39-46.

[4] N. A. Patankar and D. D. Joseph, *Modeling and numerical simulation of particulate flows by the Eulerian–Lagrangian approach*, International Journal of Multiphase Flow, Volume 27, Issue 10, October 2001, Pages 1659-1684.

[5] ANSYS Inc. *ANSYS Fluent User's Guide*,

[6] S. Pirker and D. Kahrimanovic and C. Goniva, *Improving the applicability of discrete phase simulations by smoothening their exchange fields*, Applied Mathematical Modelling, Volume 35, Issue 5, May 2011, Pages 2479-2488.

[7] P. P. Brown and D. F. Lawler, *Sphere Drag and Settling Velocity Revisited*, 3rd ed. Journal of Environmental Engineering, Volume 129, Issue 3, March 2003.

[8] S. Whitaker, *Forced convection heat transfer correlations for flow in pipes, past flat plates, single cylinders, single spheres, and flow in packed beds and tube bundles*, AIChE Journal, Volume 18, Issue 2, March 1972.

[9] P. R. Smith, *Bilinear interpolation of digital images*, Ultramicroscopy, Volume 6, Issue 2, 1981, Pages 201-204.

[10] Mathworks, *Profiler documentation*, http://mathworks.com/help/matlab/ref/profile.html.